Neuron, Vol. 23, 337–351, June, 1999, Copyright ©1999 by Cell Press

# Variability in the Time Course of Single Photon Responses from Toad Rods: Termination of Rhodopsin's Activity

**G. G. Whitlock and T. D. Lamb***
Physiological Laboratory
University of Cambridge
Downing Street
Cambridge CB2 3EG
United Kingdom

## Summary

**We examined the responses of toad rod photoreceptors to single photons of light. To minimize the effects of variability in the early rising phase, we selected sets of responses that closely matched the rise of the mean single photon response. Responses selected in this way showed substantial variations in kinetics, appearing to peel off from a common time course after different delays. Following incorporation of the calcium buffer BAPTA, the time to peeling off was retarded. Our analysis indicates that it is not necessary to invoke a long series of reaction steps to explain the shutoff of rhodopsin activity. Instead, our results suggest that the observed behavior is explicable by the presently known shutoff reactions of activated rhodopsin, modulated by feedback.**

## Introduction

In 1979, Baylor et al. showed that vertebrate rod photoreceptors can respond reliably to individual photons of light. They found that the amplitudes of the single photon responses in different trials showed a limited degree of variability, with a coefficient of variation (= standard deviation/mean) of 0.2, and they reported that the shapes of the individual responses were very similar to the shape of the mean response. Subsequently, Schnapf (1983), Schneeweis and Schnapf (1995), and Baylor (1996) have investigated the variability in response kinetics and, based mainly on analysis of the ensemble variance, have concluded that the single photon responses exhibit very little variation in shape. Most recently, Rieke and Baylor (1998) have conducted an extensive investigation of toad rod responses. Although they observed variability in the shape of the single photon responses, they interpreted the degree of reproducibility to imply that the termination of R* activity is likely to involve a series of 10–20 unidentified transitions within the rhodopsin molecule.

In this study, we also have examined the responses of toad rods to single photons, and we have found variability closely resembling that observed by Rieke and Baylor (1998). But when we analyze the recordings using a molecular model of transduction that explicitly includes the R* "lifetime," we find that in different trials, the extracted lifetime exhibits a moderately large coefficient of variation of about 0.4. From this value, a simplistic model (in which inactivation stages have fixed and equal rate constants) would suggest that the number of steps underlying R* shutoff might be about six (obtained as $0.4^{-2}$; see Discussion). However, that calculation ignores the possibility of feedback onto R* lifetime (e.g., by $Ca^{2+}$, as suggested by our results with BAPTA), and it might thereby significantly overestimate the actual number of steps. To test the model, we have carried out stochastic simulations based on the supposition that R*'s activity is shut off in a single step, and we find that this scheme predicts responses remarkably similar to the observed ones. As a result, we think that the degree of kinetic variability that is observed experimentally may be explicable simply by the presently known molecular reactions of R* inactivation: binding and phosphorylation by rhodopsin kinase (RK), followed by arrestin binding.

*To whom correspondence should be addressed (e-mail: tdl1@cam.ac.uk).

## Results

### Properties of Single Photon Responses

We recorded the electrical responses of toad rods to long series of very dim flashes that had been adjusted in intensity to deliver a mean of 0.5–1 photoisomerization per trial. Figure 1 illustrates conventional analysis of results obtained from a control cell tested with 350 dim flashes and shows that the observed behavior was closely similar to that reported in previous investigations. The sample of 50 consecutive responses in Figure 1A broadly resembles that obtained by Rieke and Baylor (1998; Figure 3B). Response "failures" are clearly visible and are fairly well separated from a group of single photon events. We presume that the four largest traces represent multiple photon hits. In Figure 1B, the histogram of response amplitudes for the entire set of trials (measured at the time to peak of the ensemble mean) demonstrates obvious quantization, as expected for the discrete nature of light absorption, and as found previously (Baylor et al., 1979, 1984; Schnapf, 1983; Schneeweis and Schnapf, 1995; Baylor, 1996; Rieke and Baylor, 1998). We shall refer to the single photon responses as "singletons."

In earlier studies, one of the main lines of evidence for the occurrence of a stereotypical waveform was the finding that the time course of the ensemble variance, $\sigma^2(t)$, is closely similar to the shape of the square of the ensemble mean response, $\mu^2(t)$ (Schnapf, 1983; Schneeweis and Schnapf, 1995; Rieke and Baylor, 1998). Figure 1D shows that we find the same result, with $\sigma^2(t)$ exhibiting a shape very similar to $\mu^2(t)$. However, we differ from previous work in proposing that this finding does not provide strong evidence for reproducibility. Although the occurrence of a stereotypical response waveform would always lead to a common shape for $\sigma^2(t)$ and $\mu^2(t)$, the converse inference cannot be drawn. For dim flashes, the variance is overwhelmingly dominated by the quantal nature of light (i.e., by the squared error between the ensemble mean and the failures), so that the occurrence of even substantial variability in

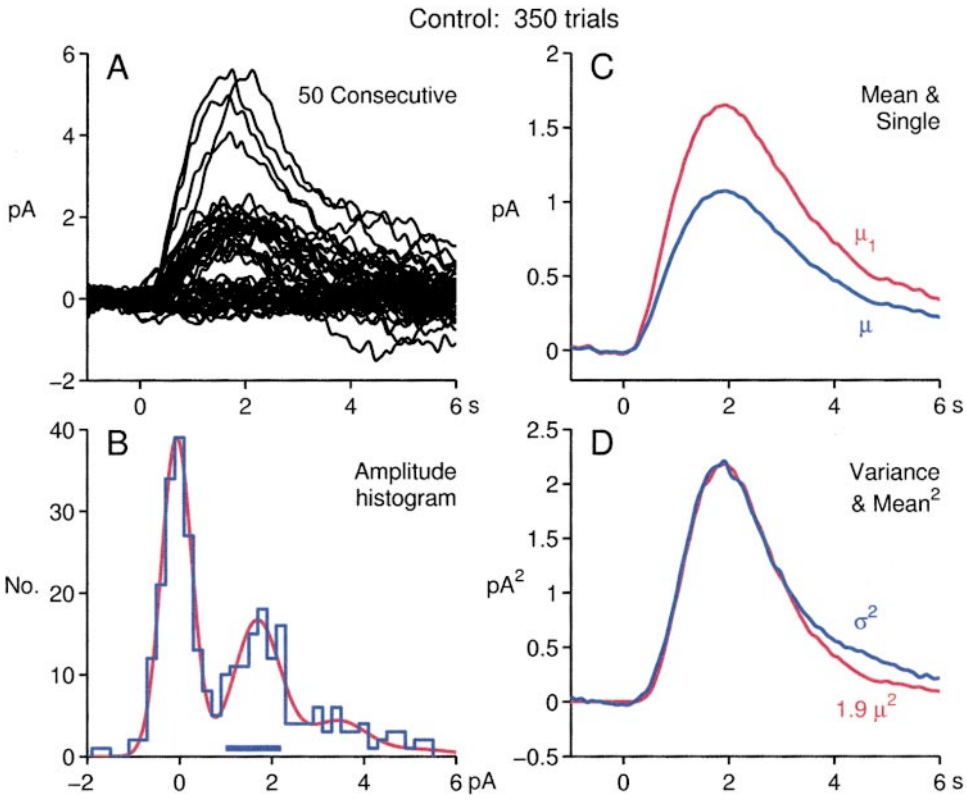


Figure 1. Conventional Analysis of Responses: Control Conditions

Responses of a toad rod under control conditions. In each trial, a brief flash was presented at time zero, delivering 0.08 photons/$\mu m^{-2}$ (20 ms; 500 nm; slit width, 16 $\mu$m), estimated to cause on average about 0.6 photoisomerizations; interval between trials, 10 s. Maximal response to bright diffuse flashes, 42 pA. The responses were filtered, and traces with poor baselines were rejected, as described in Experimental Procedures. This left 309 of the original 350 responses for analysis.

(A) Sample of 50 consecutive responses.

(B) Histogram of the amplitude distribution for the complete set of responses, measured at the time to peak of the mean response, $t = 1.9$ s. Curve is Equation 10 of Baylor et al. (1979), with $\Phi = 0.65$, $a = 1.75$ pA, $\sigma_0 = 0.33$ pA, and $\sigma_1 = 0.38$ pA. Horizontal bar shows the range of amplitudes taken in subsequent analysis as conventional singletons; there were 85 such events within the indicated range of 1–2.2 pA.

(C) Ensemble mean response, $\mu(t)$, together with estimated mean singleton response, $\mu_1(t)$, obtained as $\mu_1(t) = \mu(t)/\Phi$.

(D) Ensemble variance, $\sigma^2(t)$, compared with a scaled version of the square of the mean response, $1.9\ \mu(t)^2$.

the shape of singletons would contribute only a small component to the variance.

### Variability of Singletons Selected with a Common Rising Phase

In an ideal, noise-free experiment, simple visual inspection of the raw events ought to indicate whether the singleton waveform is stereotypical, but in real experiments (Figure 1A), the occurrence of noise meant that visual inspection did not provide a completely clear-cut answer. But in viewing the raw responses, we gained the impression that there was greater variation in the recovery phase than in the onset phase, and we suspected that variations in the gain of transduction might be camouflaging variations in the kinetics of recovery. We therefore devised a test to examine the kinetics, independent of any differences of gain in the early rising phase.

#### *Selection of Traces*

To obviate the influence of variations in transduction gain, we selected subsets of responses that closely matched the early rising phase of the mean singleton, $\mu_1(t)$. Forty traces selected in this way are illustrated in Figure 2A, and as an aid to visualization, they have been color coded into five groups, according to their amplitudes at a later time ($t = 2.5$ s, indicated by the second arrow). Quite clearly, the illustrated responses do not all exhibit the same shape. The individual responses tend to rise along a common curve (because they have been selected to do so), yet they differ in amplitude, in time to peak, in final recovery, and in area. In Figure 2B, we have averaged the colored groups of traces from Figure 2A. These averaged traces confirm the trend that is apparent in the noisy raw traces—the responses appear to break away from one another at different times, so that there is a marked tendency for larger responses to exhibit a later peak and a later final recovery. The earliest time at which the traces begin to "peel away" from a common curve is about 0.8 s.

#### *Classification of Responses*

One potential criticism of the analysis in Figure 2A is that the selected responses may not in fact be singletons. To investigate this possibility, we applied the conventional method of response classification by measuring the amplitudes of the individual responses at the time to peak of the mean response ($t = 1.9$ s, indicated by the first

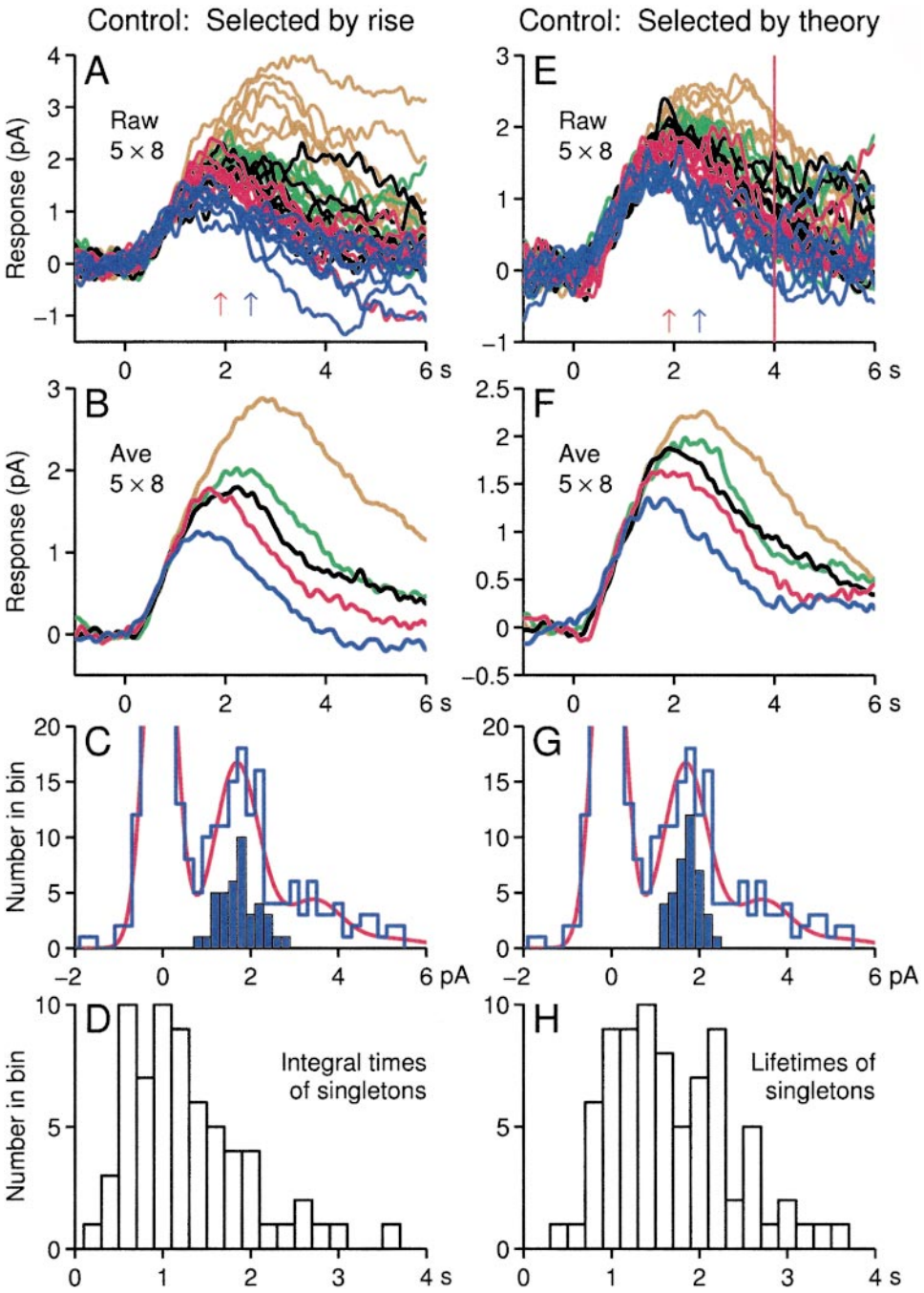


Figure 2. Variability in Kinetics of Singletons: Control Conditions

Analysis of variability in the kinetics of the singletons from the cell in Figure 1. Left column, selection of traces by early rising phase. Right column, selection based on the fit of the predictions of the model of discrete R* lifetime.

(A) The 40 responses that best matched the rise of the mean singleton at early times (−1 to 1 s) have been selected (see Experimental Procedures). These traces have been color coded into five groups, according to their amplitude at a later time (2.5 ± 0.1 s), the center of which is indicated by the second arrow (blue).

(B) Averages of the colored raw responses from (A).

(C) Amplitude distribution of the responses in (A) (closed bars), superimposed on the histogram from Figure 1B. All amplitudes were measured at the time to peak of the mean response (1.9 s), indicated by first arrow (red) in (A).

(D) Distribution of integral times, $t_{int}$. Values are plotted for responses identified as singletons after exclusion of those with a poor fit of the rising phase; this left 68 of the 85 events within the range indicated by the bar in Figure 1B.

(E) Responses (40) have been selected in order of the closeness of the gain scaling factor $r_{max}$ $A$ for the individual responses to that of the mean singleton (see text). Color coding as in (A). The vertical line at 4 s indicates the time up to which the fit was calculated and therefore gives the maximum lifetime that could be extracted.

(F) Averages of the colored raw responses in (E).

(G) Amplitude distribution of the responses selected in (E) (closed bars).

(H) Distribution of extracted lifetimes, $t_{life}$, for the singleton responses after exclusion of those with a poor fit of Equation 2; this left 78 of the 85 events within the range of the bar in Figure 1B.

arrow). As shown in Figure 2C, the amplitudes of the selected responses fell fairly neatly into the quantal peak obtained for the entire set of responses. With the possible exception of three responses (one in the leftmost bin and one in each of the rightmost two bins in Figure 2C), each of the 40 selected responses would be classified as a singleton by the conventional method. Yet because the individual responses exhibited a range of times-to-peak, their peak amplitudes showed wide variation.

***Other Possible Sources of Apparent Variability***

We applied five further tests to determine whether the variations seen in the left column of Figure 2 might have been artificial. First, to examine whether the variability might have arisen from the procedure of choosing responses that matched the unity scaling of the mean singleton response, i.e., that matched $1 \times \mu_1(t)$, we repeated the selection procedure for raw responses that were either smaller or larger, e.g., that matched $0.8\ \mu_1(t)$ or $1.2\ \mu_1(t)$. Visually, the variability in the responses selected in this way appeared just the same as that seen in responses selected to match the unity scaling of the mean, and we conclude that the variations do not result from the selection procedure. Second, to examine whether the slower recovery seen in the larger traces might have resulted from a gradual slowing of the cell's kinetics, we compiled scatter plots of response amplitude as a function of the sequence in which the responses were obtained (Whitlock, 1998). We found no significant correlation, and we conclude that the differences shown in Figure 2 do not result from a gradual change in properties. Third, we investigated whether the occurrence of spontaneous thermal isomerizations might underlie the variability; such events would be confounding if they occurred within a window of about 2–3 s during the rising phase. But as the mean interval between thermal events has been measured as 50 s (Baylor et al., 1980), only about 4%–6% of responses (2–3 s/50 s) would be expected to exhibit a spontaneous event in the susceptible period. Thus, in the 40 traces of Figure 2A, only a few responses would be expected to be affected in this way. Hence, although it is possible that several of the largest responses in Figure 2A might have been artificially increased in amplitude by the occurrence of a thermal event during the rising phase, the remaining wide degree of variation must have had a different origin. Fourth, we considered whether spatial variations in kinetics (Schnapf, 1983), even over our narrow light stimulus, could have accounted for the differences. Over the entire outer segment length of 60 μm, the time to peak increases steadily from about 1.5–2 s (Schnapf, 1983), so a variation of only 0.1–0.2 s would be expected over our stimulating slit, 16 μm wide. Furthermore, the slower responses from the tip of the outer segment have a smaller peak and therefore have a much smaller rising phase slope than the faster responses from the base (Schnapf, 1983). Hence, even if spatial variations in kinetics did occur, our procedure of matching the rising phase would have selected against the effect. Finally, we tested our selection procedure on simulated responses that were all scaled replicas of a common shape, with added noise. In this case, the selected traces displayed only minor variations (data not shown), very different from the results in Figure 2.

In summary, although there are a number of influences that could potentially contribute variability, we are confident that the basic phenomenon illustrated in Figure 2—namely, the existence of considerable variability in the kinetics of the recovery of singletons—is real.

## Quantitative Measures of the Variability in Recovery Kinetics

***Integral Time***

To provide a quantitative measure of the kinetic variability, we measured the area under the individual singleton traces, normalized by the gain of the individual early rising phase (as described in the Experimental Procedures). If the singletons all exhibited identical shape and varied only in amplitude, then we would expect this parameter (which we term the "integral time," $t_{int}$) to be constant. The measured distribution of $t_{int}$ is plotted in Figure 2D for the 68 singletons obtained in this experiment (after exclusion of responses that were poorly fit over their rising phase, 68 responses remained from the 85 that would conventionally be classified as singletons; see legend). This histogram shows that the kinetics of the individual singletons display wide variations. The integral time, $t_{int}$, ranged from about 0.5 s to at least 2 s, with a mean of 1.24 s and a coefficient of variation (ratio of standard deviation to mean) of $cv = 0.57$. Such a large coefficient of variation indicates that the individual responses exhibit considerable differences in shape.

***Fitting of Kinetic Models***

In their recent analysis, Rieke and Baylor (1998) found variability in the kinetics of singletons, which they quantified by fitting a model having four hypothetical stages of recovery, each with the same time constant, τ. For this four-equal-stage case, the predicted shape of the flash response is

$$r_{equal}(t) = c\left(\frac{t}{\tau}\right)^3 \exp\left(-\frac{t}{\tau}\right), \qquad \text{for } t > 0, \tag{1}$$

where $c$ is a scaling factor. Application of this kinetic model to the experimental results yielded a relatively narrow distribution for the τs of singletons, with a coefficient of variation of $cv(\tau) \approx 0.2$ (Rieke and Baylor, 1998). As shown below, we obtained similar results when we applied the same analysis to our data.

In addition, we have analyzed the singletons using a molecular model, extended from the recent kinetic analysis of Nikonov et al. (1998), of the shutoff reactions in the transduction cascade. In their Equation 19, Nikonov et al. formulated a scheme with three distinct molecular mechanisms of shutoff: R* inactivation (with a time constant, $\tau_{R^*}$), G*–PDE* inactivation (with a time constant, $\tau_E$), and recovery of cyclic GMP (cGMP) concentration (with a time constant, $\tau_\beta$). We have assumed that for a given cell, the latter two mechanisms are reproducible in different trials and that what varies between trials is the shutoff of R*. Furthermore, in order to determine whether the results might be explicable by just a single stochastic stage of R* shutoff, we extended the Nikonov et al. (1998) analysis to the case in which R* exhibits discrete "all-or-nothing" activity, with a lifetime, $t_{life}$. For this discrete lifetime model, the singleton response, $r_{discrete}(t)$, is predicted to be the response to a step "on"

minus the response to a delayed step "off," or

$$r_{\text{discrete}}(t) = r_{\text{step}}(t) - r_{\text{step}}(t - t_{\text{life}}). \quad (2)$$

The step response, $r_{\text{step}}(t)$, is obtained by the substitution of $\tau_{R^*} = 0$ into Equation 19 of Nikonov et al. (1998) as

$$r_{\text{step}}(t) = r_{\text{max}} A \left(1 - \frac{\tau_1 e^{-t/\tau_1} - \tau_2 e^{-t/\tau_2}}{\tau_1 - \tau_2}\right)\tau_1\tau_2, \text{ for } t > 0. \quad (3)$$

Here, $\tau_1$ and $\tau_2$ denote the time constants of the two inactivation reactions other than R* decay (i.e., $\tau_E$ for inactivation of PDE* and $\tau_\beta$ for recovery of cGMP). But since this expression is symmetric in $\tau_1$ and $\tau_2$, it is irrelevant which corresponds to $\tau_E$ and which to $\tau_\beta$. Note that a slightly different form applies for the case in which $\tau_1 = \tau_2$ and that, for simplicity, a short delay term of $t_{\text{eff}} \approx$ 50 ms has been omitted. The product $r_{\text{max}} A$ in Equation 3 is a scaling factor for the gain of transduction, where $A$ is the amplification constant of the outer segment (Lamb and Pugh, 1992) and $r_{\text{max}}$ is the cell's maximal response.

Using the two kinetic models above, we have been able to extract from any given set of singletons the individual values for (1) the time constant $\tau$ in the four-equal-stage model and (2) the R* lifetime $t_{\text{life}}$ in the discrete model, which minimize the mean square error in fitting the individual responses (see Experimental Procedures). Several examples of the fit of the two models are illustrated in Figure 3. In each example, the green trace plots the fit of the four-equal-stage model (Equation 1), while the red trace plots the fit of the discrete model (Equations 2 and 3) with the extracted R* lifetime $t_{\text{life}}$, indicated by the red arrow. The curve-fitting was performed over the time interval from −1 to 4 s (indicated by the vertical red line). This meant that thermal events occurring after 4 s did not distort the fitting (see second trace from top). Over the full set of trials, we found that the two models described the responses almost equally well. The discrete model exhibited a rather abrupt recovery, with long values of $t_{\text{life}}$ (see upper two traces), that was not always apparent in the responses, while on many occasions, the four-equal-stage model exhibited a peak that appeared broader than the real response. For the cell illustrated, the residual variance over all the singletons was 0.034 pA$^2$ for the four-equal-stage model and 0.039 pA$^2$ for the discrete lifetime model.

***Fitting as an Alternative Means of Selection of Traces***

Application of the discrete lifetime model provided a second means of selecting singletons that rose with a common time course, and results selected in this way are illustrated in the right-hand column of Figure 2. The 40 selected traces in Figure 2E have been chosen according to two criteria. First, ~10% of outliers were rejected on the basis of a poor fit of the theory curve. Thus, a trial was rejected if the residual variance (the variance of the difference between the response and its best-fitting theory trace) exceeded some limit, which for this cell was 0.10 pA$^2$ (i.e., about 2.5 times the mean residual variance). In practice, this criterion removed those trials that appeared to contain a spontaneous thermal event. From the remaining responses, the selection of traces was made in order of the closeness of the

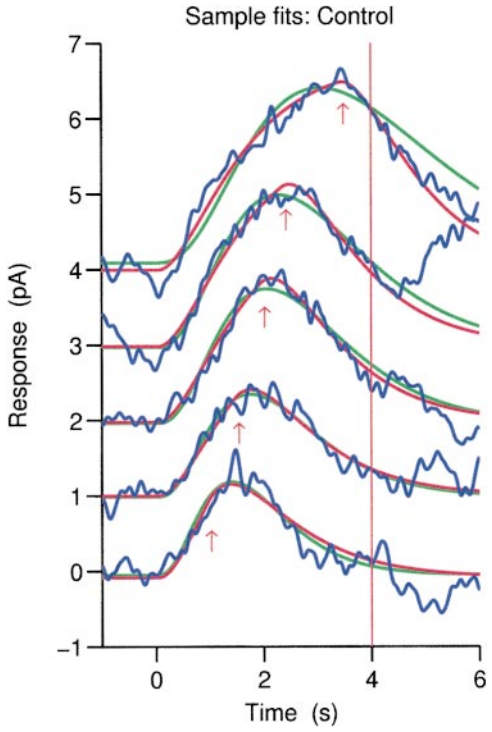


Figure 3. Sample Singleton Responses Fitted with the Two Kinetic Models

Five sample singletons are shown from the experiment in Figure 2 to illustrate the fit of the two different kinetic models. In each case, the green trace shows the fit of the four-equal-stage formulation, expressed by Equation 1, and the red trace shows the fit of the model of discrete R* lifetime, expressed by Equations 2 and 3. The arrows indicate the best-fitting R* lifetime, $t_{\text{life}}$. The interval over which the traces were fit extended from −1 to 4 s (indicated by the vertical line). The traces have been offset by intervals of 1 pA for clarity.

gain scaling factor ($r_{\text{max}} A$) of individual trials to the scaling factor for the mean singleton.

This second method of selecting a subset of singletons is therefore closely analogous to the first method, and it provides a check on the form of the selected responses. The difference between the two methods is that in the first approach (Figure 2, left column), the individual traces were chosen according to the scaling of the ensemble mean at early times (typically until 1 s after the flash), whereas in the second approach (Figure 2, right column), the traces were selected according to the scaling of the theoretical expression over a longer interval (typically until 4 s after the flash). In both cases, the traces were selected in order of the closeness of their scaling factors to that of the mean singleton. A comparison of Figures 2A and 2E shows that the selected traces are broadly similar—in fact, 20 of the 40 selected traces are common to the two panels. However, because the second approach rejects traces that are poorly fit by the equation at later times, it avoids the selection of some of those traces in Figure 2A that appear (by visual inspection) to contain a spontaneous thermal event subsequent to the flash.

For the responses selected by this second method, we examined the amplitude distribution measured at

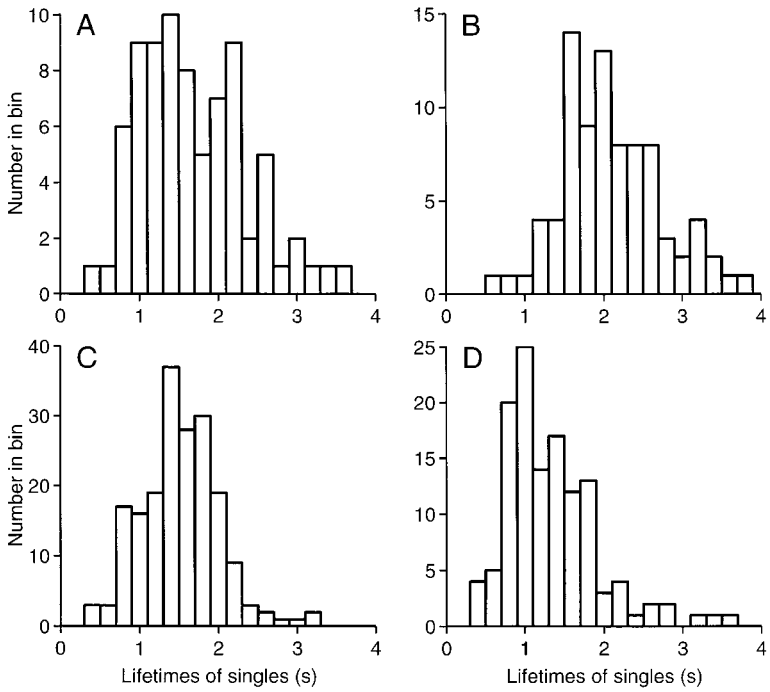


Figure 4. Distribution of Extracted Lifetimes for Singletons: Control Cells

Collected distributions of extracted singleton lifetime, $t_{life}$, for the four control cells that were held long enough to obtain at least 300 stable dim flash responses. Each panel is comparable to Figure 2H. For the four cells, the total number of trials, the estimated mean number of photons per trial ($\Phi$), the interflash interval, the circulating dark current, the number of singleton events that were well-described by Equation 2, the mean value of $t_{life}$, and the coefficient of variation of $t_{life}$ were as follows. (A): 350 trials, $\Phi = 0.65$, 10 s intervals, 42 pA dark current, 78 singletons, mean $t_{life} = 1.70$ s, $cv = 0.40$; (B): 357 trials, $\Phi = 0.90$, 8 s intervals, 27 pA dark current, 84 singletons, mean $t_{life} = 2.11$ s, $cv = 0.30$; (C): 750 trials, $\Phi = 0.82$, 8–10 s intervals, 28 pA dark current, 190 singletons, mean $t_{life} = 1.52$ s, $cv = 0.33$; and (D): 425 trials, $\Phi = 1.1$, 8 s intervals, 18 pA dark current, 125 singletons, mean $t_{life} = 1.34$ s, $cv = 0.45$.

the time to peak of the ensemble mean response (1.9 s). The resulting narrow peak in Figure 2G clearly corresponds to the singleton's peak of the entire ensemble, as obtained by conventional analysis. Hence, all of the selected traces in Figure 2E were singletons.

### *Lifetime Distribution*

Application of this kinetic model provided estimates for the lifetime of R*, and Figure 2H shows the distribution of extracted lifetimes over the 78 singletons in this experiment that were well fitted (i.e., that appeared not to exhibit a spontaneous thermal event). The distribution is quite broad, and the extracted values are spread over a range of at least 0.8–3 s. The mean extracted lifetime was 1.70 s, and the standard deviation was 0.68 s, giving a coefficient of variation for the hypothetical R* lifetime of $cv(t_{life}) = 0.40$. This is slightly smaller than the earlier result, in which the integral times in Figure 2D were distributed with $cv(t_{int}) = 0.57$. A likely reason for the difference is that the estimates of integral time are inflated by noise in the recordings.

### *Collected Results*

We found variability of the kind illustrated in Figures 1–3 in each of four control cells held for long enough to obtain at least 300 "stable" responses; by stable, we mean that over the course of the experiment (typically 2 hr), the amplitude of the cell's bright flash response changed by $<15\%$, the mean time to peak changed by $<10\%$, and there were no visible signs of deterioration. In cells recorded with fewer than about 300 stable responses, there were usually insufficient traces remaining after the selection procedure to be certain of the existence of the effect, given the levels of recording noise. Nevertheless, in five of a further six control cells recorded with at least 100 stable responses, variability of the same qualitative kind clearly appeared to be present, and in no cell did we obtain the impression that the response shape might be invariant.

Collected results for the extracted lifetimes are plotted in Figure 4 in the four control cells recorded with at least 300 dim flash trials. In each case, the distribution of lifetimes is quite broad, with values spread over a ratio of at least 2:1. For the four cells, the coefficient of variation of the extracted lifetime, $cv(t_{life})$, was 0.40, 0.30, 0.33, and 0.45 (mean, 0.37). For these same cells, the coefficient of variation of the integral time, $cv(t_{int})$, as determined by the approach in the left column of Figure 2, was 0.57, 0.41, 0.35, and 0.52 (mean, 0.46). Together, these findings indicate that the singletons exhibit substantial variations in kinetics.

### *Correlation between Fitted Values of $\tau$ and $t_{life}$*

Figure 5 plots the correlation that we found between the fitted values for $\tau$ in the four-equal-stage model and the fitted values for the hypothetical R* lifetime $t_{life}$ in the discrete model. For each of the four control cells, the correlation was very high, with $r^2 > 0.95$, and in each case the intercept of the regression line with the ordinate occurred at $\tau \approx 0.3$–$0.4$ s; i.e., at a positive value. As a result, the coefficient of variation for $\tau$ was always smaller than that for $t_{life}$, with a ratio typically of $cv(\tau) \approx \frac{1}{2} cv(t_{life})$. For the four cells illustrated, $cv(\tau)$ was 0.21, 0.18, 0.14, and 0.19 (mean, 0.18), close to the value of 0.21 ($= 1/4.8$) reported by Rieke and Baylor (1998) but about half the mean value of $cv(t_{life}) = 0.37$, obtained above. The systematic difference between the coefficients of variation for $\tau$ and $t_{life}$ presumably arises from the assumption implicit in the four-equal-stage formulation that all four time constants vary in unison; quantitatively, that assumption would be expected to reduce $(cv)^2$ by a factor of roughly 4 (see Discussion), and the observed reduction was close to this. Hence, we conclude that by fitting the experimental results with a model of four equal stages, the coefficient of variation is underestimated by a factor of about 2 from the value

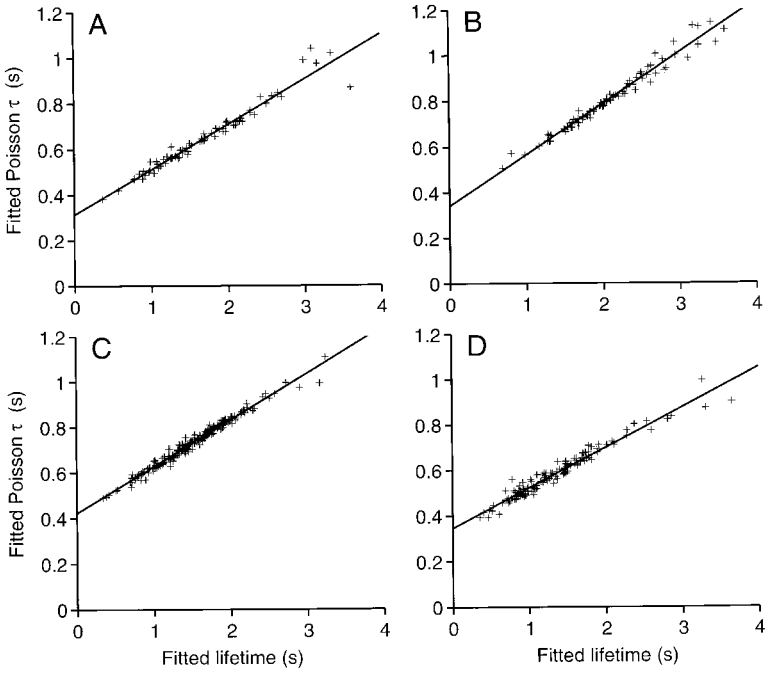


Figure 5. Correlation of Four-Equal-Stage Time Constant with R* Lifetime: Control Cells

Plots of the correlation between the extracted values of the time constant $\tau$ (using the four-equal-stage equation) and the R* lifetime $t_{life}$ (using the discrete model) for the same four cells as in Figure 4. Each symbol represents an individual singleton (and corresponds to one bin count in Figure 4), and the straight lines plot the calculated linear regression. For the four cells, the slope, vertical intercept, and correlation coefficient of the regression lines were as follows. (A): slope 0.20, intercept 0.31 s, $r^2 = 0.96$; (B): slope 0.22, intercept 0.34 s, $r^2 = 0.97$; (C): slope 0.20, intercept 0.42 s, $r^2 = 0.98$; and (D): slope 0.18, intercept 0.35 s, $r^2 = 0.95$. In the four panels, the coefficients of variation of $\tau$ and of $t_{life}$ and the ratio of these parameters were as follows. (A): $cv(\tau) = 0.21$, $cv(t_{life}) = 0.40$, ratio 0.53; (B): $cv(\tau) = 0.18$, $cv(t_{life}) = 0.30$, ratio 0.59; (C): $cv(\tau) = 0.14$, $cv(t_{life}) = 0.33$, ratio 0.43; and (D): $cv(\tau) = 0.19$, $cv(t_{life}) = 0.45$, ratio 0.42.

that would be obtained if the kinetic variability arose from changes in the lifetime of a single inactivation step.

**Variability in Transduction Gain of the Singletons**

Our method of fitting the individual responses with the kinetic model of discrete lifetimes provides a means of investigating variability in the gain of transduction, as well as variability in the kinetics. Figure 6A plots the distribution we obtained for the gain scaling factor $r_{max} A$ for the cell illustrated in Figures 1–3 and clearly shows the existence of a quantal peak. The smooth curve has exactly the same form as the curve previously fit to the conventional histograms of amplitude distribution and was obtained with $cv(r_{max} A) = 0.13$. As the rod's circulating dark current shows little variability, we assume that differences in the scaling factor $r_{max} A$ arise predominantly from variations in the amplification constant of transduction $A$, perhaps as a result of variations in the packing density of proteins in the different discs in which the photoisomerizations occurred in different trials.

To investigate a possible link between the gain scaling factor and the response kinetics, Figure 6B plots the averaged responses obtained for different magnitudes of the gain scaling. Thus, each trace in the panel is the average response for groups of trials that yielded gain scaling factors centered either at zero or at integer multiples of 1.5 pA $s^{-2}$. Importantly, this panel shows that the time to peak shortens as the gain scaling factor increases (indicated approximately by the sloping line). Furthermore, this acceleration occurs within the singleton's group, as shown by the third, fourth, and fifth traces from the bottom. The responses to double (or triple) hits are further accelerated, to the extent that the recovery phases of the larger traces fold back over those for intermediate traces (indicated by the U-turn arrow). An important consequence of this acceleration is that at late times, the singleton and double-hit responses are much more similar to each other than they are near the peak, so that the ensemble variance will be less than predicted on simple models. This acceleration is presumably caused by the dynamic reduction in $Ca^{2+}$ concentration during the flash response. It effectively represents a manifestation of light adaptation at the single photon level.

In Figure 6C, we have plotted the conventional estimates of response amplitude (measured at the peak of the ensemble mean response) against the new estimates of gain scaling factor, and we find that there is quite a high correlation ($r^2 = 0.86$). The visual impression elicited by the point plot of Figure 6C is to some extent weakened by the clustering of points into failures and singletons. Therefore, in Figure 6D, we have determined the density of the points and presented the results as a pseudocolor density plot. The results in these two panels show that the conventional approach and the new approach each generate a very similar allocation of trials into failures, singletons, and multiple hits.

**Effect of Increased Cytoplasmic Calcium Buffering**

To examine the possible role of cytoplasmic $Ca^{2+}$ concentration in the variability of the singleton kinetics, we incorporated the calcium buffer BAPTA into the cytoplasm via its acetoxymethyl ester (AM) (Matthews, 1991). Figure 7 shows results analogous to those in Figures 1 and 2 for a cell tested with 499 dim flashes after incorporation of BAPTA. The sample of 50 consecutive responses in Figure 7A shows a grouping into failures, singletons, and what appear to be "doubles," although (as in Figure 1A) the boundaries are not entirely clear-cut; in addition, there are one or two larger responses. For the entire set of trials, the histogram in Figure 7B (measured at the peak of the mean response, $t = 4$ s) shows a prominent failure's peak together with a singleton's peak that is about twice as broad as in control

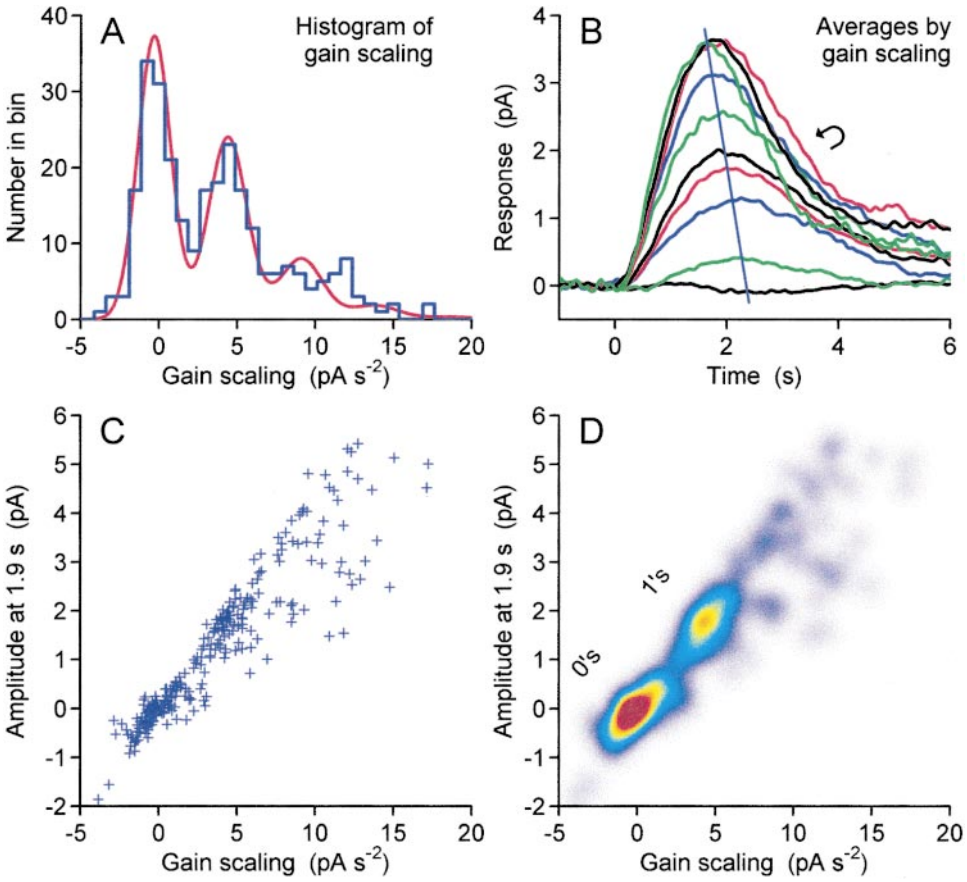


Figure 6. Distribution of Gain Scaling Factor $r_{max}$ *A* and Correlation with Amplitude

(A) Histogram showing the distribution obtained for the gain scaling factor $r_{max}$ *A* in Equation 3, when the model of discrete R* activity was fit to the responses of the cell in Figures 1–3. The smooth curve is the Poisson-weighted sum of Gaussians (as used in Figures 1, 7, and 9) with the following parameters: $\Phi = 0.65$, $\mu_1 = 4.7$ pA s$^{-2}$, $\sigma_0 = 1.05$ pA s$^{-2}$, and $\sigma_1 = 0.63$ pA s$^{-2}$.

(B) Sets of averages of individual responses that had gain scaling factors in different bins. Bin widths were 1.5 pA s$^{-2}$ centered at zero and at integer multiples of 1.5 pA s$^{-2}$. Thus, the third, fourth, and fifth traces from the bottom corresponded to small, medium, and large responses within the singletons' peak. Note that averaged responses that rise more rapidly reach peak earlier, as indicated approximately by the sloping line.

(C) Correlation between the new measure of gain scaling factor $r_{max}$ *A* (abscissa) and the conventional measure of amplitude at the time to peak of the mean response (ordinate). The correlation coefficient was $r^2 = 0.86$. Note that the histogram count in any bin in (A) represents the number of symbols (trials) vertically below that bin in (C); likewise, the conventional amplitude histogram of Figure 1B would correspond to the vertical axis in (C).

(D) Pseudocolor plot of the density of points in (C). Each point from (C) was replaced by a two-dimensional Gaussian function (with $\sigma_x = \sigma_y =$ 2.5% of the full-scale axes), and these functions were summed; this procedure corresponds to two-dimensional convolution with a Gaussian. The existence of the two relatively sharp peaks indicates that the two approaches agree quite well in identifying failures and singletons; however, there is less consistency in the assignment of multiple hits.

cells (coefficient of variation, $cv(a) = 0.35$, compared with a mean of $cv(a) = 0.20$ in control cells). As in control cells, the ensemble variance, $\sigma^2(t)$, exhibits a waveform closely similar to that of the ensemble mean response squared, $\mu^2(t)$, at least up until the peak (Figure 7C). Hence, apart from the slower responses and the broader singleton's peak in the histogram, the behavior seen in these conventional tests on cells containing BAPTA is qualitatively similar to that seen in control cells.

Figure 7D shows traces that have been selected to closely match the early rising phase of the mean single photon response, $\mu_1(t)$. Sixty raw responses are illustrated, color coded into five groups of 12, according to their amplitude at $t = 5$ s (Figure 7D, second arrow). As in Figure 2, it is clear that the responses do not all share the same shape, and this is confirmed by the averaged traces plotted in Figure 7E. With BAPTA in the cytoplasm, the earliest time at which traces began "peeling-off" from each other was around 1.5 s, considerably later than in the control cell (0.8 s). Similarly, the integral times, $t_{int}$ (Figure 7F), were shifted to larger values, ranging from about 3 to 6 s; the mean $t_{int}$ was 4.44 s, and its standard deviation 1.02 s, giving a coefficient of variation of $cv(t_{int}) = 0.23$.

We also analyzed the responses of this cell using the model of discrete R* activity to extract the hypothetical lifetime of the activated R* in each trial. The responses selected by this method were similar to those illustrated in Figures 7D and 7E (with 33 of the 60 traces being common), and therefore, further panels analogous to the right column of Figure 2 have not been illustrated. The extracted lifetimes ranged from about 2.5 to 5.5 s,

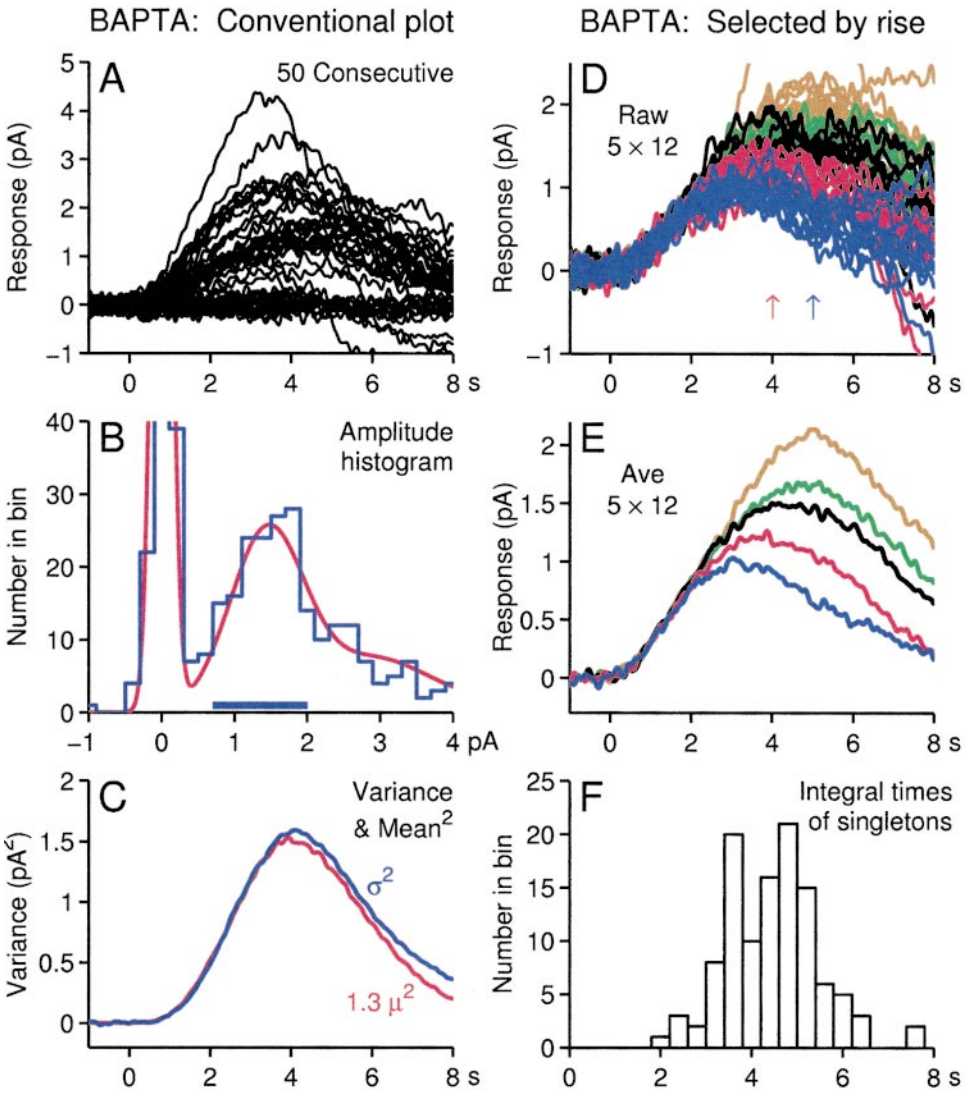


Figure 7. Variability in Response Kinetics: Rod Containing BAPTA

Responses of a rod in which the calcium buffer BAPTA had been incorporated. Flashes at time zero delivered 0.09 photons/$\mu m^{-2}$ (20 ms; 500 nm; slit width, 16 $\mu$m), estimated to cause an average of about 0.7 photoisomerizations per flash. Circulating dark current, 22 pA. Responses were filtered, and those with poor baselines were rejected as previously, leaving 448 of the original 499 responses for analysis. Left column, conventional analysis. Right column, selected responses and distribution of integral times.

(A) Sample of 50 consecutive raw responses. Right column, selected responses and distribution of integral times.

(B) Histogram of the amplitude distribution for the complete set of responses, measured at the time to peak of the mean response, $t = 4$ s; the vertical scale has been expanded in order to show the singletons' peak more clearly. Curve is Equation 10 of Baylor et al. (1979) with $\Phi = 0.78$, $a = 1.45$ pA, $\sigma_0 = 0.12$ pA, and $\sigma_1 = 0.50$ pA.

(C) Ensemble variance, $\sigma^2(t)$, compared with a scaled version of the square of the mean response, $1.3\ \mu(t)^2$.

(D) The 60 responses that best matched the rise of the mean single photon response at early times ($-1$ to 2 s) have been selected (see Experimental Procedures). Traces are color coded into five groups of 12, according to their amplitude at a later time ($5 \pm 0.1$ s), indicated by the second (blue) arrow.

(E) Averages of the colored raw responses from (D).

(F) Distribution of integral times, $t_{int}$, for the singletons. After exclusion of those with a poor fit of the rising phase, 112 events remained from the 139 within the range of 0.7–2 pA, indicated by the bar in (B). In experiments with BAPTA, the flashes were delivered at variable intervals, according to whether or not the preceding flash had elicited a response (see Experimental Procedures). Therefore, the failure traces in (A) have been truncated after the minimum interflash interval of 4 s in those trials in which the subsequent flash elicited a response; in calculating the mean and variance, the subsequent portions of those traces were assigned as zero.

with a mean of 3.87 s and a standard deviation of 0.87 s, giving a coefficient of variation of $cv(t_{life}) = 0.22$.

For each of four BAPTA-containing cells held for sufficiently long to record at least 300 stable dim flash responses, we obtained results closely similar to those in Figure 7. In addition, for five of a further seven BAPTA-containing cells recorded with at least 100 responses, the results were qualitatively similar, despite the small numbers of traces remaining after the selection procedure. In these cells, the electrogenic $Na^+/Ca^{2+}$ exchange

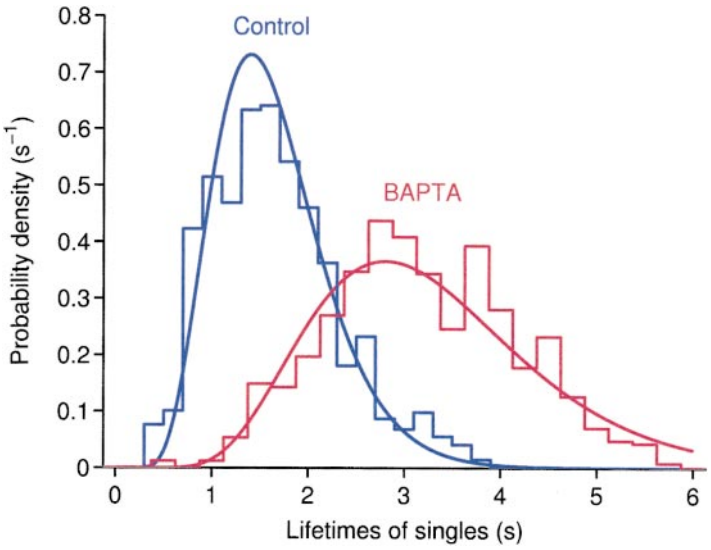


Figure 8. Comparison of Extracted Lifetimes: Control Versus BAPTA

Averaged histograms for distributions of extracted lifetime. The histograms were averaged from the two groups of four cells that were each held long enough to obtain at least 300 stable dim flash responses; blue for four control cells, red for four cells containing BAPTA. Because of the different numbers of single photon responses recorded for each cell, the individual histograms were converted to units of probability density (i.e., fraction of total responses in each bin, divided by bin width) before they were averaged. The blue curve plots Equation 5 with $n = 6$, $\tau = 0.24$ s, and $t_0 = 0.2$ s. This function was found to provide a reasonable fit to the measured lifetime distribution, and therefore, its integral (Equation 6) was used in generating the simulated responses. The red curve plots the same function, except that $\tau$ and $t_0$ have both been doubled. For the control cells, the circulating currents were given in the legend to Figure 4; for the cells containing BAPTA, the circulating currents were 22 pA, 20 pA, 21 pA, and 24 pA.

current was monitored with saturating flashes (Yau and Nakatani, 1985) and was found to be slowed by a factor of 2–5× (the time constant typically increased from 0.6 s to about 2 s), indicating significant buffering of cytoplasmic $Ca^{2+}$ concentration.

The distributions of extracted R* lifetimes are plotted in averaged form in Figure 8 from the four control cells and the four cells containing BAPTA for which we were able to record at least 300 stable dim flash responses. Clearly, the average distribution of lifetimes for the cells containing BAPTA (Figure 8, red) is shifted to the right relative to that for the control cells (Figure 8, blue). This finding parallels two earlier observations: that the peeling-off times of the traces were later for BAPTA cells (Figures 7D and 7E) than for control cells (Figures 2A and 2B) and that the integral times, $t_{int}$, were substantially increased (compare Figure 7F with Figure 2D).

### Stochastic Simulations

Given that we have been able to apply a model of discrete R* activity to the experimental data and thereby to extract and plot the distribution of hypothetical R* lifetimes, it is natural to ask whether stochastic simulations would generate responses with properties resembling those of real responses. In other words, can a model of R* shutoff through a single stochastic step account for the observed behavior?

Before beginning simulations, we first needed to specify the probability distribution of R* lifetimes, $p(t_{life})$, in our model, and to do this, we employed an arbitrary curve that provided a reasonable fit to the histogram in Figure 8. We then generated a set of stochastic lifetimes that were pseudorandomly distributed in accordance with this probability density function. From these values of $t_{life}$, we calculated the individual simulated responses using Equations 2 and 3, and finally, we added simulated noise. Details are given in the Experimental Procedures.

Figure 9 shows an analysis of the responses simulated with this stochastic scheme, using the same methods that we applied to the responses of real cells, and it illustrates that the simulations exhibit many of the features of real responses. Thus, the simulated responses show substantial variability in kinetics (Figures 9D and 9E), with a coefficient of variation for $t_{int}$ of about 0.38 (Figure 9F); the amplitude histogram shows clear quantization (Figure 9B); and the ensemble variance has a time course broadly similar to the square of the mean response (Figure 9C).

One apparent difference between the simulated and real responses is that by visual inspection (Figure 9A), the simulated responses appear more variable in their recovery phase than do the real responses (Figure 1A). Correspondingly, the ensemble variance exceeds the mean squared response at relatively late times (Figure 9C). However, we think that part of this apparent discrepancy might arise from our neglect in this simplified model of the dynamic acceleration of guanylyl cyclase activity that is induced by the normal drop in $Ca^{2+}$ concentration during the light response. As we showed in Figure 6B, the average double-hit response and the average singleton response are more nearly similar to each other at late times than would be expected from simple scaling of the entire time course. This type of phenomenon would reduce the variance at late times. In any case, the results in Figure 9 indicate that a simple stochastic model of all-or-nothing R* activity can come quite close to describing the observed behavior.

## Discussion

### Variability in Single Photon Response Kinetics

Our results show that significant variations occur in the time course of single photon responses, both in control cells and in cells that have had BAPTA incorporated into the cytoplasm. Singleton responses that have been selected to match along their early rising phase appear to peel away from each other at different times after the flash. The responses reach peak at different times and therefore attain different peak amplitudes, and they exhibit considerable differences in the time to final recovery.

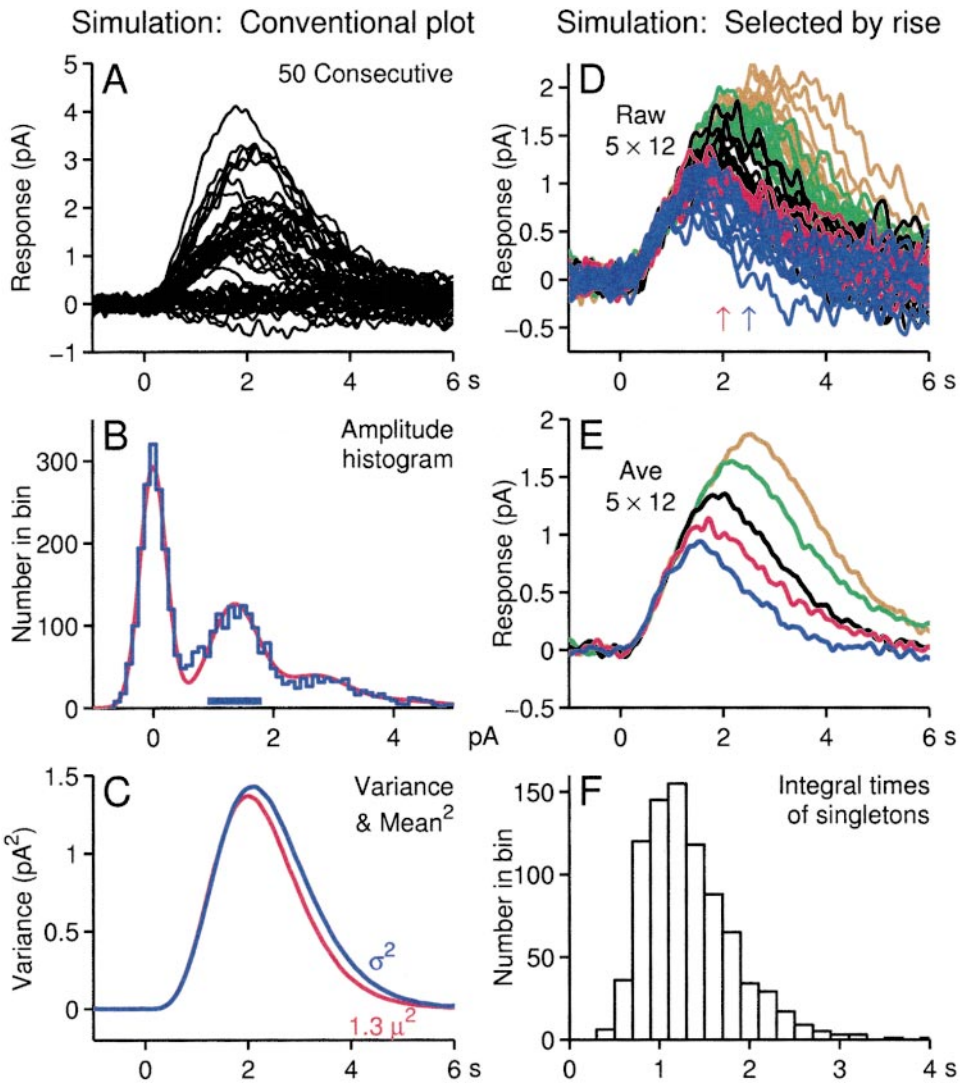


Figure 9. Kinetic Variability of Responses Simulated with Stochastic Model of R* Activity

Responses obtained by stochastic simulation of the model of discrete R* activity have been analyzed as previously. Left column, conventional analysis. Right column, selected responses and distribution of integral times.

(A) Sample of 50 consecutive simulated responses.

(B) Amplitude distribution for all 4000 simulated responses. Parameters of curve: $\Phi = 0.8$, $a = 1.35$ pA, $\sigma_0 = 0.22$ pA, and $\sigma_1 = 0.35$ pA.

(C) Ensemble variance, $\sigma^2(t)$, compared with a scaled version of the square of the mean response, $1.3\ \mu(t)^2$.

(D) Simulated responses (60) selected to match the rise of the mean response at early times. For realistic comparison with Figure 2, only the first 500 of the 4000 simulations were considered. First (red) arrow indicates time to peak of the ensemble mean response. Responses are color coded into five groups of 12, according to their amplitude at 2.5 s, indicated by the second (blue) arrow.

(E) Averages of the five colored groups from (A).

(F) Distribution of integral times, $t_{int}$, for singletons; the mean was 1.33 s, and the coefficient of variation 0.38. Of the 938 events identified as singletons (with amplitudes in the range of 0.9–1.8 pA, indicated by the bar in [B], 102 were rejected on the basis of excessive variance in the fit of the rising phase, leaving 836 events for inclusion in the histogram of integral times.

In contrast, previous investigators have reported that the singletons exhibit very little variation in kinetics (Baylor et al., 1979, 1984; Schnapf, 1983; Schneeweis and Schnapf, 1995; Baylor, 1996; Rieke and Baylor, 1998). Thus, Rieke and Baylor (1998) refer to the remarkable "reproducibility" of the responses and report that "the entire shape of the elementary response was also nearly constant across trials" (p. 1841). In fact, our data are closely similar to theirs, but our interpretation differs significantly. The difference is not merely semantic—whether the bottle is half-full or half-empty—but is instead a substantive issue, upon which hinges the set of possible molecular mechanisms that could underlie the shutoff of photoactivated rhodopsin.

We confirmed the conventional findings that the amplitudes of the singletons (measured at the time to peak of the ensemble mean response) exhibit a coefficient of variation of $cv(a) \approx 0.2$ and that the shape of the ensemble variance is closely similar to that of the square of the ensemble mean. Furthermore, when we fitted the four-equal-stage kinetic model used by Rieke and Baylor (1998), we found a coefficient of variation for the time constant of $cv(\tau) \approx 0.2$, a value indistinguishable from the one they obtained.

In addition, we fitted a kinetic model based on the known shutoff stages of the phototransduction cascade (Nikonov et al., 1998). The two fitting procedures are very similar, in that both involve four delay stages: on the one hand, four equal (but hypothetical) time constants; on the other hand, R* lifetime, G*–PDE* decay time constant, cGMP recovery time constant, and a short time delay of $t_{eff} \approx 0.05$ s. The main difference between the two is that in the former case, all four time constants are required to change in unison, whereas in the latter case, only one parameter—the R* lifetime—changes in different trials. When we applied this molecular model, the coefficient of variation that we obtained for the extracted R* lifetime, $cv(t_{life}) \approx 0.4$, was approximately double the value for the four-equal-stage model, $cv(\tau) \approx 0.2$. The difference in estimates of *cv* almost certainly arises from the fact that in the four-equal-stage model, the four time constants vary in unison, whereas in our molecular description, only a single stage—the R* lifetime—varies between trials.

### Role of $Ca^{2+}$ Concentration

Our results with incorporation of calcium buffer are also similar to those obtained by Rieke and Baylor (1998) with exposure to $Ca^{2+}$ clamping solution. In both studies, it was found that the amplitude histogram was still quantized and that the shape of the variance was again the same as that of the squared mean response. However, our interpretation again differs from theirs. Although Rieke and Baylor argued that their results indicated that the reproducibility of the kinetics was essentially unchanged in the absence of $Ca^{2+}$ feedback, they did not in fact directly measure the variability of the individual single photon kinetics under clamped conditions. We do not accept that the amplitude histogram (measured at the time to peak of the mean response) provides definitive evidence for the presence or absence of variations in kinetics. Nor do we think that comparison of the ensemble variance with the mean squared response provides a conclusive test for the occurrence of variations in kinetics of the quantal events, since the bulk of the variance is contributed by the squared difference between the ensemble mean response and the failures; i.e., by the quantal nature of photon absorption.

To directly study the variability of response kinetics in cells containing BAPTA, we examined the individual responses to single photons. As in the case of control cells, we again found pronounced variations, but three aspects of the timing were retarded in comparison with control cells. First, by visual inspection, it appeared that the range of times over which the responses peeled away from each other was considerably later (compare Figures 2B and 7E); second, the integral times were roughly doubled in cells containing BAPTA; and third, the extracted estimates of R* lifetime were also approximately doubled (Figure 8). These changes from the normal behavior have convinced us that $Ca^{2+}$ plays a key role in triggering the termination of R* activity in control cells.

We suggest that a likely reason for the different interpretations of the role of $Ca^{2+}$ in the two studies is that Rieke and Baylor's (1998) tests were sensitive primarily to fractional (rather than to absolute) changes in kinetic variability. Consider what would happen if $Ca^{2+}$ clamping were to lead to a doubling of the standard deviation of the variability in R* shutoff kinetics but were also to lead to a doubling of the time to peak of the flash response (in part through effects on guanylyl cyclase). We think that in this case, there would be negligible change in the shape of the amplitude histogram and in the relationship between ensemble variance and ensemble mean squared response, such that their tests would presumably detect no change.

A noticeable feature of the averaged traces in Figures 2B and 2F is their resemblance to the effects of adaptation by very weak backgrounds. Since it is known that light adaptation is associated with reduced cytoplasmic $Ca^{2+}$ concentration (Matthews et al., 1988; Nakatani and Yau, 1988), a potential contributory factor in the variability of recovery times in control cells would be the occurrence of fluctuations in the resting $Ca^{2+}$ concentration at the location and time of photon absorption as a result of the "continuous" component of noise (Baylor et al., 1980; Rieke and Baylor, 1996). If the longitudinal localization of internal messengers effectively divides the outer segment into about ten independent regions (each about 6 μm long in a 60 μm outer segment; Lamb et al., 1981), then the fluctuations recorded by the suction pipette will be reduced (in fractional terms) by a factor of $\sqrt{10}$ from the underlying fluctuations in local current. The observed fluctuations have an rms amplitude of about 0.2 pA (Baylor et al., 1980), corresponding to a peak-to-peak excursion of up to 1 pA in a dark current of 15–25 pA (see Baylor et al., 1980, Figure 7; Leibrock et al., 1994, Figure 1). Thus, after spatial averaging, the peak-to-peak continuous noise corresponds to about 4% of the dark current, such that locally, the peak-to-peak current fluctuations would represent about 12% of the circulating dark current and would induce fluctuations in $Ca^{2+}$ concentration of about the same fractional size. Fluctuations of this magnitude might have appreciable effects on the kinetics of the single photon responses.

### Number of Stages Involved in R* Shutoff

Rieke and Baylor (1998) reported that the variance within the singletons was about 15–20 times smaller than the ensemble variance, and they used this as the basis for estimating the number of stages involved in R* shutoff to be 10–20 (their Figure 18). However, their analysis was based on two assumptions: first, that the amplitude histogram provides an unambiguous means of selecting all the single photon events, with no possibility of misclassification, and second, that the single photon responses are entirely independent of the preexisting baseline level, such that a time-dependent baseline variance can be subtracted. In our view, there are difficulties with both of these assumptions. Thus, the absence of extreme singletons would be expected to lead to a general underestimate of the variance, while the subtraction of a time-varying baseline variance might have reduced the variance artificially at later times (see Rieke and Baylor, 1998, Figure 5). Accordingly, we think that the small signal (<10% of the ensemble variance), extracted for the "variance within singletons," is of limited accuracy.

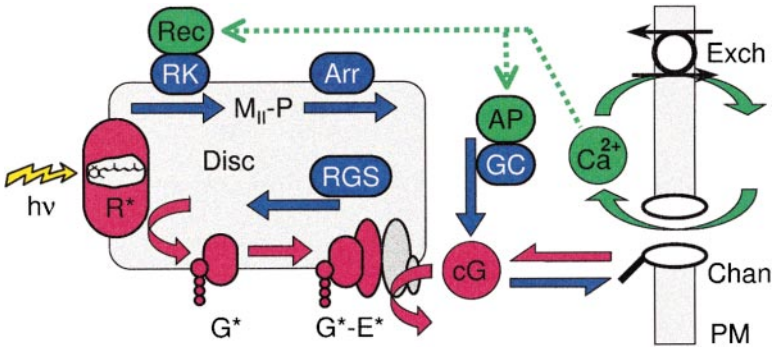


Figure 10. Molecular Schematic of the Reactions of Phototransduction

Species and steps are colored red for activation, blue for inactivation, green for regulation. For activation, a photon (hν) isomerizes rhodopsin to its active form R*, now identified as metarhodopsin II ($M_{II}$). R* catalyzes activation of a G protein to G*, which binds to an effector E protein, activating it to G*−E*. The effector is a phosphodiesterase, which hydrolyzes cGMP (cG) in the cytoplasm, leading to closure of ion channels at the plasma membrane (PM). For inactivation, R* binds RK and is phosphorylated to form $M_{II}$−P. Arrestin (Arr) then binds, substantially completing the inactivation of R*. G*−E* is inactivated by hydrolysis of the terminal phosphate of Gα−GTP, a reaction accelerated by an RGS protein (regulator of G protein signaling; He et al., 1998) that is probably complexed to the type 5 G protein β subunit (Gβ5; Makino et al., 1999). The inactive G and E then separate. cGMP is continually formed by guanylyl cyclase (GC). For regulation, closure of channels causes a drop in cytoplasmic $Ca^{2+}$ concentration, regulating the cascade in (at least) two locations. GC activity is modulated by an activating protein (AP) (Gorczyca et al., 1994). RK activity is modulated by recoverin (Rec) (Kawamura, 1993; Klenchin et al., 1995; Tanaka et al., 1995). For further discussion of the reactions, see Nikonov et al. (1998).

Another approach would be to consider the magnitude of the coefficient of variation of the kinetics, as was originally done for the coefficient of variation of the amplitudes by Baylor et al. (1979). In general terms, the coefficient of variation resulting from a chain of $n$ stochastic reactions will be of the order of $(cv)^2 \approx 1/n$ if each rate constant is of similar magnitude. Substituting our mean value of $cv(t_{life}) \approx 0.37$, we obtain a rough estimate for the required number of shutoff stages as $(1/0.37)^2$, or about 7, subject to the proviso that these hypothetical stages have constant parameters. However, the actual number of stages involved might be much smaller than this if their rate constants are not constant—for example, if feedback occurs onto one or more of the stages.

In view of these findings, we have asked: what is the minimum number of stages that must be invoked in the shutoff of R* in order to account for the observed variability in kinetics? And as an extreme: is it possible that termination of R* activity in a single step could explain the results? To examine this question, we undertook simulations of a model of stochastic R* shutoff, and we found that the simulated responses (Figure 9) were closely comparable to the behavior of real cells. From this finding, we conclude that it is not in fact necessary to invoke a long series of stepwise reductions in the activity of an individual R* molecule in order to account for the experimental results. Instead, we think that the experimental results are likely to be explicable by a scheme in which R* is inactivated by the presently known reactions, as explained below.

## Possible Molecular Mechanism

The known reactions of transduction are summarized in schematic form in Figure 10. As is well documented, the shutoff of R* is mediated initially by the interaction of R* with RK, and subsequently, by the binding of arrestin (Wilden et al., 1986). In our analysis and modeling, we adopted the extreme assumption that the activity of R* is totally shut off in a single reaction step—yet even this extreme assumption provided a surprisingly accurate account, both of the individual response kinetics (Figure 3) and of the overall variability (Figure 9). In reality, we think that more than one molecular step is likely to be involved. Thus, the binding of RK may cause partial inactivation (Pulvermüller et al., 1993), and phosphorylation may cause partial inactivation (Miller et al., 1986; Wilden et al., 1986), while arrestin binding appears likely to cause substantially complete inactivation (Wilden et al., 1986).

Our interpretation of the lifetime histograms in Figures 4 and 8 is that R* does not exhibit a fixed lifetime but that instead, the rate constant of R* inactivation increases with time. A prime candidate molecule for mediating an increase in the rate constant of R* shutoff would be RK, and two distinct mechanisms are likely to contribute. First, we think that feedback plays a significant role, and, as originally suggested by Torre et al. (1986), we think that one of the feedback messengers is $Ca^{2+}$. Thus, we propose that the local drop in $Ca^{2+}$ concentration during the single photon response shortens the R* lifetime, most probably through the Ca-dependent decline in binding of recoverin to RK, which should steadily increase the amount of RK available for binding and phosphorylating R* as $Ca^{2+}$ declines (Kawamura, 1993; Klenchin et al., 1995). Second, we suggest that activation of RK by R* during the light response (Fowles et al., 1988) might also play an important role.

In addition to the effects on R* lifetime, any intermolecular interactions that appeared to render R*'s activity graded would lead to more reproducible single photon response kinetics. For example, if the binding between RK and R* were rapidly reversible, then as the amount of RK available for binding increased, R* would appear to exhibit gradually declining activity. Similarly, a local accumulation of GDP (as G* is activated) might gradually reduce the apparent activity of R*. Taken in combination, it seems entirely plausible to us that modulation of R* lifetime and activity by established mechanisms could reduce the overall variability in single photon kinetics to the degree actually observed.

## Conclusions

In summary, our recordings show that the single photon responses of rod photoreceptors are not stereotypical in shape but that instead, they appear to inactivate over

a range of times—a tendency that is delayed when changes in calcium concentration are slowed down. We see no necessity in invoking a series of 10–20 hypothetical reactions in the shutoff of activated rhodopsin to account for the observations. Instead, we think that the measured variability is likely to be explicable in terms of the presently known reactions underlying termination of R* activity: namely, the interactions of R* with the G protein, with RK, and with arrestin, in conjunction with feedback mediated at least in part by $Ca^{2+}$ and recoverin. The main difference between our interpretations and those of Rieke and Baylor (1998) is that we think the observed variability in kinetics is likely to be caused by interactions of R* with other molecules, rather than by a series of intramolecular rearrangements. We plan to investigate quantitatively whether a detailed molecular model along these lines is capable of explaining all of the experimental observations.

## Experimental Procedures

### Electrical Recordings and Flash Delivery

Toads, *Bufo marinus*, were dark adapted overnight and then killed by decapitation and pithing. Electrical responses of isolated rods were recorded with a suction pipette by using the methods of Lamb et al. (1986). To minimize the contribution of spatial variations in transduction parameters (Schnapf, 1983), the light stimuli (500 nm, 20 ms duration) were restricted to a region 16 μm wide at the middle of the outer segment. A long series of very dim flashes was presented, adjusted in intensity to deliver a mean of typically $\Phi = 0.5$–1 photoisomerizations per flash, as determined from light calibrations and from the proportion of response failures.

Responses were filtered DC–20 Hz and were then digitally low-pass filtered, usually at 2.5 Hz. To reject traces containing spurious noise (possibly due to spontaneous thermal events), an automated procedure was devised. Specifically, the response baseline (the period of 1 s prior to the flash) was tested, and the response was rejected if the mean slope lay outside set bounds (usually ±2 standard deviations) or if the variance exceeded a set limit (typically 0.015 $pA^2$). This led to the rejection of 10%–15% of the original set of traces. No responses were rejected manually.

In experiments in which BAPTA was incorporated, the cells were incubated in AM, according to the method of Matthews (1991). To increase the number of trials in the BAPTA experiments, during which the responses recovered slowly, the flashes were delivered at variable intervals. Thus, if one flash elicited a failure, then the next flash was delivered after a short interval (4 or 5 s), whereas if it elicited a response, then the next flash was not delivered until the first response had recovered, typically after 12 or 15 s. For display of traces from these experiments (see Figure 7), the failure traces have been truncated after the minimum interflash interval in those cases in which the subsequent flash elicited a response. In calculating the mean and variance, the failure traces were set to zero after that time.

### Conventional Histogram Analysis and the Mean Single Photon Response

The amplitude of an individual response was taken as the difference between the average level over two windows: a baseline window (1 s wide, immediately prior to the flash) and a measurement window (0.2–0.4 s wide, centered at the time to peak of the mean dim flash response). The amplitudes were binned, and the Poisson-weighted Gaussian expression, Equation 10 of Baylor et al. (1979), was then fitted. The four parameters of this equation are $\Phi$, $a$, $\sigma_0$, and $\sigma_1$, where $\Phi$ is the mean number of photoisomerizations per flash, $a$ is the mean single photon response amplitude (at the peak), $\sigma_0^2$ is the variance of the failures' peak, and $\sigma_1^2$ is the additional variance in the singletons' peak. The mean singleton response, $\mu_1(t)$, was obtained from the ensemble mean response as $\mu_1(t) = \mu(t)/\Phi$ (see Figure 1C), since $\mu(t) = \Phi\ \mu_1(t)$, provided that the singletons add linearly.

### Calculation of Variance

We calculated the ensemble variance at each instant of time using the raw traces (as described by Baylor et al., 1979), and the plotted variance is shown as the change from the mean preflash level. In contrast, Rieke and Baylor (1998) adopted a different approach by first clamping the individual preflash baseline levels to zero and subsequently subtracting an estimate of the "time-dependent baseline variance." Despite this difference, the qualitative form of the variance traces is remarkably similar in the two studies. It is possible, though, that Rieke and Baylor's approach might underestimate the variance within singletons (see above).

### Selection of Subsets of Singletons Matching the Rise of the Mean Single Photon Response

The mean singleton response, $\mu_1(t)$, was fitted to the individual raw responses by the least-squares criterion (Baylor et al., 1979) over a window covering the first half of the rising phase. Thus, the individual scaling factors, $c_i$, and offsets, $d_i$, were determined for the fit of $c_i\mu_1(t) + d_i$ to the $i$th raw trace, over $-1\ s < t < t_{end}$, where the end time $t_{end}$ was typically 1 s for control cells and 2 s for cells containing BAPTA. To minimize the contribution of thermal isomerizations and other transients, we used an automatic procedure to exclude from subsequent analysis the 10%–15% of responses that gave the poorest fits; thus, we excluded the traces with the largest residual variance in the fitting process above.

Traces for display (in Figures 2, 7, and 9) were then selected in order of the closeness of $c_i$ to the desired scaling (usually unity). A second method (not illustrated) gave very similar results. Responses were selected in order of their goodness of fit from among those values of $c_i$ that fell close to the desired scaling (typically within ±20%).

### Integral Time

We measured the area under the individual traces by integrating with respect to time. To obtain a parameter independent of the gain of transduction, we normalized the area by the amplitude of the individual response at an early reference time; specifically, we used the amplitude (at $t_{ref} = 1$ s) of the scaled response $c_i\mu_1(t)$, which had been fitted to the early rising phase. Normalized in this way, the area had dimensions of time. Finally, we scaled this parameter by a fixed factor of 1/4 in order to bring the values to about the same magnitude as the times of peeling-away in Figures 2 and 7. Thus, for the $i$th response, we determined the integral time, $t_{int}$, defined by

$$t_{int} = \frac{\int r_i(t)dt}{4\ c_i\mu_1(t_{ref})}. \quad (4)$$

where the range of integration was 0–6 s.

To determine the distribution of integral times for singletons, we first needed to select all those events that we could be reasonably sure were "singles." To do this, we first specified an amplitude range, within the histogram of amplitude distributions, that encompassed most of the singletons yet avoided possible "small doubles" or "large failures" (see bar in Figure 1B). We selected all of the events within this range, except those that had been excluded above on the basis of the poor fit of the scaled mean to the rising phase.

### Extraction of R* Lifetimes by Analysis of Singletons

We determined the individual lifetimes of discrete R* activity that provided the best description of each of the raw traces by fitting Equations 2 and 3 to the individual responses. Thus, for each response, $r_i(t)$, we determined the best-fitting value of $t_{life}$. We used the function *fmin* in Matlab (The Mathworks, Natick, MA) to find $t_{life}$ that minimized the residual sum-of-squares difference between $r_i(t)$ and $r_{discrete}(t)$. In doing this, we required values for the two recovery time constants, $\tau_1$ and $\tau_2$, representing recovery of G*−E* and of cGMP concentration. In control cells, we found that the tail phase of the individual responses was well-described with two time constants, each close to 1 s. Since the decay of G*−E* is not expected to change in the presence of BAPTA, we therefore held one of the

time constants fixed (at $\tau_1 = 1$ s) for all cells, and we found the value of the other time constant ($\tau_2$) needed to provide a good fit to the tail phase of the individual responses. In control cells, this second time constant ranged from 0.67 to 1.25 s, while in cells containing BAPTA, it ranged from 1.25 to 2 s. The program displayed the individual responses together with the fitted traces so that the operator could check that the fitting appeared reasonable.

**Simulated Responses**

We generated simulated responses by using an assumed form for the probability density distribution $p(t_{life})$ of R* lifetimes. The density function chosen (which had no particular significance) was

$$p_{life}(t) = \frac{1}{n!\tau}\left(\frac{t - t_0}{\tau}\right)^{n-1} \exp\left(-\frac{t - t_0}{\tau}\right), \qquad \text{for } t > t_0. \tag{5}$$

In fitting this relation to the experimentally determined distribution, we chose an exponent of $n = 6$, a time constant of $\tau = 0.24$ s, and a time shift of $t_0 = 0.2$ s. The resulting trace for $p_{life}(t)$ is plotted as the blue curve in Figure 8. Integration of $p_{life}(t)$ in Equation 5 gives the cumulative probability function, $Pr_{inact}(t)$ (i.e., the probability that the R* has inactivated by time ($t$), as

$$Pr_{inact}(t) = 1 - \exp\left(-\frac{t - t_0}{\tau}\right) \sum_{i=0}^{n} \frac{1}{i!}\left(\frac{t - t_0}{\tau}\right)^{i}, \qquad \text{for } t > t_0. \tag{6}$$

We simulated 4000 individual R* lifetimes, $t_{life}$, by generating a set of pseudorandom numbers (*rand*), uniformly distributed in the interval 0–1, and then solving $Pr_{inact}(t_{life}) = rand$ numerically with the Matlab *fzero* function. Individual simulated responses were then obtained with Equations 2 and 3, with $\tau_1 = 1$ s and $\tau_2 = 0.67$ s, and with the short transduction delay set to $t_{eff} = 0.05$ s. In Figure 6, we found variability in the gain scaling factor $r_{max}$ $A$. Hence, $A$ was simulated as having a coefficient of variation of $cv = 0.12$ about its mean. The mean value of the product $r_{max}$ $A$ in Equation 2 was taken as 3.4 pA $s^{-2}$ (e.g., $r_{max} = 28$ pA and mean $A = 0.12$ $s^{-2}$).

Finally, to simulate the baseline recording noise, two components of Gaussian-distributed fluctuations were added, representing, first, thermal noise in the leakage resistance between the suction pipette and the outer segment ($\sim$5 M$\Omega$), with a spectral density of 0.003 $pA^2$/Hz (Baylor et al., 1979, Figure 9), and second, the continuous component of photoreceptor noise, with a spectral density of 0.15 $pA^2$/Hz over a bandwidth of DC–0.15 Hz (see Baylor et al., 1980).

**Acknowledgments**

We wish to thank E. N. Pugh, Jr. for many helpful discussions and suggestions during the project and F. Rieke and D. A. Baylor for helpful comments on an earlier version of the manuscript. This work was supported by grants from the Wellcome Trust (034792, 045453).

Received March 10, 1999; revised May 5, 1999.

**References**

Baylor, D.A. (1996). How photons start vision. Proc. Natl. Acad. Sci. USA *93*, 560–565.

Baylor, D.A., Lamb, T.D., and Yau, K.-W. (1979). Responses of retinal rods to single photons. J. Physiol. *288*, 613–634.

Baylor, D.A., Matthews, G., and Yau, K.-W. (1980). Two components of electrical dark noise in toad retinal rod outer segments. J. Physiol. *309*, 591–621.

Baylor, D.A., Nunn, B.J., and Schnapf, J.L. (1984). The photocurrent, noise and spectral sensitivity of rods of the monkey *Macaca fascicularis*. J. Physiol. *357*, 575–607.

Fowles, C., Sharma, R., and Akhtar, M. (1988). Mechanistic studies of the phosphorylation of photoexcited rhodopsin. FEBS Lett. *238*, 56–60.

Gorczyca, W.A., Gray-Keller, M.P., Detwiler, P.B., and Palczewski, K. (1994). Purification and physiological identification of a guanylate cyclase activating protein from retinal rods. Proc. Natl. Acad. Sci. USA *91*, 4014–4018.

He, W., Cowan, C.W., and Wensel, T.G. (1998). RGS9, a GTPase accelerator for phototransduction. Neuron *20*, 95–102.

Kawamura, S. (1993). Rhodopsin phosphorylation as a mechanism of cyclic GMP phosphodiesterase regulation by S−modulin. Nature *362*, 855–857.

Klenchin, V.A., Calvert, P.D., and Bownds, M.D. (1995). Inhibition of rhodopsin kinase by recoverin. Further evidence for a negative feedback system in phototransduction. J. Biol. Chem. *270*, 16147–16152.

Lamb, T.D., and Pugh, E.N., Jr. (1992). A quantitative account of the activation steps involved in phototransduction in amphibian photoreceptors. J. Physiol. *449*, 719–758.

Lamb, T.D., McNaughton, P.A., and Yau, K.-W. (1981). Spatial spread of activation and background desensitization in toad rod outer segments. J. Physiol. *319*, 463–496.

Lamb, T.D., Matthews, H.R., and Torre, V. (1986). Incorporation of calcium buffers into salamander retinal rods: a rejection of the calcium hypothesis of phototransduction. J. Physiol. *372*, 315–349.

Leibrock, C.S., Reuter, T., and Lamb, T.D. (1994). Dark adaptation of toad rod photoreceptors following small bleaches. Vision Res. *34*, 2787–2800.

Makino, E.R., Handy, J.W., Li, T.S., and Arshavsky, V.Y. (1999). The GTPase activating factor for transducin in rod photoreceptors is the complex between RGS9 and type 5 G protein β subunit. Proc. Natl. Acad. Sci. USA *96*, 1947–1952.

Matthews, H.R. (1991). Incorporation of calcium chelator into guinea-pig rods shows that calcium mediates mammalian photoreceptor light adaptation. J. Physiol. *436*, 93–105.

Matthews, H.R., Murphy, R.L.W., Fain, G.L., and Lamb, T.D. (1988). Photoreceptor light adaptation is mediated by cytoplasmic calcium concentration. Nature *334*, 67–69.

Miller, J.L., Fox, D.A., and Litman, B.J. (1986). Amplification of phosphodiesterase activation is greatly reduced by rhodopsin phosphorylation. Biochemistry *25*, 4983–4988.

Nakatani, K., and Yau, K.-W. (1988). Calcium and light adaptation in retinal rods and cones. Nature *334*, 69–71.

Nikonov, S., Engheta, N., and Pugh, E.N., Jr. (1998). Kinetics of recovery of the dark-adapted salamander rod photoresponse. J. Gen. Physiol. *111*, 7–37.

Pulvermüller, A., Palczewski, K., and Hofmann, K.P. (1993). Interaction between photoactivated rhodopsin and its kinase: stability and kinetics of complex formation. Biochemistry *32*, 14082–14088.

Rieke, F., and Baylor, D.A. (1996). Molecular origin of continuous dark noise in rod photoreceptors. Biophys. J. *71*, 2553–2572.

Rieke, F., and Baylor, D.A. (1998). Origin of reproducibility in the responses of retinal rods to single photons. Biophys. J. *75*, 1836–1857.

Schnapf, J.L. (1983). Dependence of the single photon response on longitudinal position of absorption in toad rod outer segments. J. Physiol. *343*, 147–159.

Schneeweis, D.M., and Schnapf, J.L. (1995). Photovoltage of rods and cones in the macaque retina. Science *268*, 1053–1056.

Tanaka, T., Ames, J.B., Harvey, T.S., Stryer, L., and Ikura, M. (1995). Sequestration of the membrane-targeting myristoyl group of recoverin in the calcium-free state. Nature *376*, 444–447.

Torre, V., Matthews, H.R., and Lamb, T.D. (1986). Role of calcium in regulating the cyclic nucleotide cascade of phototransduction in retinal rods. Proc. Natl. Acad. Sci. USA *83*, 7109–7113.

Whitlock, G.G. (1998). Single-photon responses of toad rod photoreceptors. PhD thesis, University of Cambridge, Cambridge, United Kingdom.

Wilden, U., Hall, S.W., and Kühn, H. (1986). Phosphodiesterase activation by photoexcited rhodopsin is quenched when rhodopsin is phosphorylated and binds the intrinsic 48-kDa protein of rod outer segment. Proc. Natl. Acad. Sci. USA *83*, 1174–1178.

Yau, K.-W., and Nakatani, K. (1985). Light-induced reduction of cytoplasmic free calcium in retinal rod outer segment. Nature *313*, 579–582.